Bitlis Eren Üniversitesi Fen Bilimleri Dergisi
BİTLİS EREN UNIVERSITY JOURNAL OF SCIENCE
ISSN: 2147-3129/e-ISSN: 2147-3188
VOLUME: 13 NO: 4 PAGE: 1233-1246 YEAR: 2024
DOI: 10.17798/bitlisfen.1543679

Computational Fluid Dynamics (CFD) Analysis of 3D Printer Nozzle Designs

Rasul HAJILI[1], Mikail TEMIREL[1*]

[1]*Abdullah Gul University, School of Engineering, Mechanical Engineering Department, Kayseri, Türkiye*
(ORCID: 0009-0002-2363-3225) (ORCID: 0000-0002-8199-0100)

Keywords: 3D printing, nozzle design, computational fluid dynamics (CFD), CFD analysis, printing quality, innovation.

Abstract
Additive manufacturing, particularly 3D printing, has gained significant attention recently due to its flexibility, precision, and sustainability. Among the various 3D printing technologies, Fused Deposition Modeling (FDM) stands out as one of the most popular due to its affordability, ease of use, and print quality. However, a major drawback of FDM-based 3D printers is their relatively low print resolution. One of the key factors influencing print quality is the nozzle design, especially its geometry. As a result, numerous studies in literature have focused on improving 3D printing performance by optimizing nozzle design. In this study, we investigated the effects of nozzle geometry from a Computational Fluid Dynamics (CFD) perspective, examining three aspects: die angle, outlet size, and outlet shape. The CFD analysis revealed that the die angle primarily influences the shear stress within the nozzle, while the outlet size has a significant impact on velocity and pressure difference. The outlet shape affects shear stress, velocity, and pressure difference to a lesser extent than the die angle and size.

1. Introduction

3D printing is a type of additive manufacturing technique. This technology creates objects from a computer aided design (CAD). 3D printing process occurs by the layer-by-layer approach to build a 3D object. 3D printing is widely used in the world nowadays and it is a fast-emerging technology[1]. Industries such as aerospace employ 3D printing technology since it is achievable to create desired lightweight structures[2]. However, improvements in this field are necessary to increase the precision of the printing process to avoid additional finishing procedures and ensure efficient manufacturing.

Fused deposition modeling (FDM) is one of the popular branches of additive manufacturing. The FDM method is a common process where a filament of material is fed onto a heated bed using roller mechanism. The material is extruded through a temperature-controlled nozzle[3, 4]. In the FDM process, polymer thermoplastic filaments are commonly used by melting and extruding them through a nozzle, layer by layer, to create the final product[1]. Choosing materials for the filament and nozzle is crucial for 3D printing technology. The most common materials used in FDM are polylactic acid (PLA), acrylonitrile butadiene styrene (ABS), polypropylene (PP), and polyethylene (PE)[1]. According to the literature[5], compared to polylactic acid (PLA), acrylonitrile butadiene styrene (ABS) has higher tensile strength, Young's modulus, elongation at break, and impact strength in fused deposition modeling. Likewise, nozzle materials with high mechanical properties such as durability, low abrasiveness, and most importantly high thermal conductivity are desirable for additive manufacturing.

Properties and the effects of the flowing fluid can be studied by the method called Computational Fluid Dynamics (CFD). This is a branch of fluid dynamics that is widely used in various engineering fields. Since the equations governing fluid motion are usually too complex to be handled effortlessly using

*Corresponding author: mikail.temirel@agu.edu.tr
Received: 04.09.2024, Accepted: 29.12.2024

analytical methods, especially for complicated geometries, numerical approaches are necessary to lower the cost and computational time. CFD combines numerical analysis and computational software to solve complex fluid-related problems[6, 7]. CFD is a science based on the governing laws of fluid dynamics. It produces comprehensive predictions of fluid-flow phenomena. In addition to fluid flow, the problems involving heat transfer, mass transfer, and chemical reactions can be studied using CFD[7, 8]. Methods such as finite-difference, finite-element, spectral, and spectral element are often used in CFD to discretize and solve the system of algebraic Navier-Stokes equations. However, the results from the CFD studies must be interpreted carefully since errors are possible depending on the flow conditions and numerical methods[9, 10]. One of the examples of CFD's extensive use in R&D is in the aerospace field, where it helps to analyze flow's behavior on specified domains with various boundary conditions[11]. Consequently, it allows engineers to detect and fix design errors early on. Beyond aerospace and automotive industries, CFD is also significant in 3D printing industries as it attracts increasing interest for its practical applications[12]. Furthermore, CFD is popular as a cost-effective alternative that delivers highly accurate results compared to experimental methods.

Within the field of 3D printing, CFD has been a valuable tool for testing various printing parameters, including nozzle speed, shear stress, printability, and pressure distribution. Conducting these tests repeatedly through experiments can be both costly and time-consuming, but CFD reduces the number of necessary repetitions, making the research process more efficient. For example, new nozzle design or new filament used in printability experiments is expensive, but CFD allows researchers to study the flow behaviors and material deformation under stress computationally. In one study, COMSOL Multiphysics software was used for a comparative study of a syringe and screw-based 3D food printer to investigate and compare the flow field characteristic of 3D extrusion-based printing units[13]. Other CFD software like ANSYS POLYFLOW, COMSOL, Abaqus, and FLOW-3D have also been employed to investigate additional design parameters and nozzle configurations[14, 15]. In other study, CFD was employed to investigate the print fidelity for polyvinyl alcohol (PVA) material in extrusion dependent 3D printer to investigate the velocity, pressure, shearing rate, and viscosity distributions in nozzle[16]. Another CFD example with Ansys Fluent, focusing on the comparison of the validity of the CFD and experimental data of various parameters of solar still, conducted by Panchal and Patel[17], when the results of CFD were compared with experimental results, the outcome showed that there was a great amount of agreement. CFD is often utilized in nozzle studies, including the rocket nozzles to examine the velocity and pressure of the flowing fluid for the specified region, and the wall shear forces acting on the nozzle surface. Alamu et al.[18] showed that CFD can be applied to the analysis of printed rocket nozzles by simulating flow conditions, thereby enhancing rocket engine performance. CFD helps to characterize and estimate flow types including laminar flows[19], creeping flows (Reynold number <1)[20, 21], turbulent flows[12], non-Newtonian flows[22] as well as heat and mass transfer[8]. This is crucial for designing nozzle geometry. In particular, laminar flow is typical for most 3D printing processes, especially when using materials like thermoplastics in filament-based printers (FDM). Additionally, CFD can be performed to analyze the characteristics of the 3D printed and finalized products that are subjected to internal or external flows. CFD is also used in bioprinting, which is a branch of 3D printing[23-25]. For example, it can be used to analyze the nozzle design for interactions between bioink characteristics and nozzle designs on cell viability. COMSOL was used in a study to compare the impact of shear stress on cell viability between cylindrical and conical nozzles[26]. In the study by Fareez et al.[27], bioprinting research, CFD is performed to optimize the bioprinting by analyzing the properties such as shear stress, diffusivity, and cell viability to aid in the nozzle design and material selection.

Nozzle design can significantly influence the printing quality and durability of the nozzle material. According to Zhang and Sanjayan[28], extrusion resistance affects nozzle design and consequently 3D printing quality. Lower outlet velocity and shorter nozzle designs can enhance printing quality by reducing resistance. Additionally, the nozzle outlet diameter influences 3D printing quality by affecting tensile strength. Smaller nozzle diameters improve strength through finer layers and better adhesion but may increase printing time[29]. Another study by Kaplan et al[30]. reveals that nozzle modifications in FDM printing reduce travel movements while improving printing quality by allowing toolpath optimization, resulting in increased efficiency. Moreover, Xu et al.[31] indicates that nozzle design in 3D printing significantly affects printing speed and the surface texture of the finalized product. Nevertheless, material choice is crucial for mechanical properties.

The use of CFD is increasingly popular in the design and optimization of 3D printer nozzles. Specifically, for FDM-based 3D printers, nozzle design and printing resolution can be optimized using fluid mechanics principles, as the melted filament within the nozzle behaves like a liquid[32]. CFD provides significant benefit to the field by decreasing the cost, increasing the resolution, and fastening 3D printer developing procedure. In a study, color mixing of an FDM 3D printer nozzle was simulated in terms of filament feed with different temperature and experimentally supported[33]. CFD was also employed to simulate different types of melted thermoplastic filaments in 3D printer nozzle. As an example, carbon fiber-reinforced polymer composites were studied to assess clogging problems using CFD and the discrete element method (DEM), focusing on different fiber lengths, fiber volume fractions, and resin viscosities. The analysis revealed that nozzle clogging tends to occur when either the fiber length or the fiber volume fraction is increased[34]. In a separate study, molten TNT/HMX-based explosives were analyzed using CFD to examine the impact of pressure, nozzle diameter, viscosity, and particles on the printing process. The findings showed that increasing the nozzle diameter and inlet pressure enhances the printing velocity, whereas higher viscosity reduces the printing speed[35]. Another CFD study was conducted for the fidelity analysis of the 3D printer using polyvinyl alcohol (PVA) material in two different nozzle diameters. The findings indicated that as the shear rate increased and the gel viscosity decreased, the material could be successfully extruded from both nozzles. Additionally, the larger diameter nozzle demonstrated better performance compared to the smaller one[16]. Alphonse et al.[36] demonstrated that analyzing the outlet flow behavior using CFD can significantly aid in optimizing the performance of a 3D-printed ABS nozzle aerator design. In summary, the use of CFD for optimizing nozzle designs and finalizing 3D-printed nozzle products is a widespread practice.

However, there is a lack of studies specifically focused on simulating the diverse geometry of 3D printer nozzles. For instance, die angle and outlet geometry and their effects on the nozzle performance were not widely analyzed. Furthermore, the combined effect of outlet diameter, die angle, and outlet geometry on essential properties such as pressure drop, outlet velocity, and wall shear stress are yet to be explored. This study aims to address these gaps by utilizing Computational Fluid Dynamics (CFD) analysis and simulating the flow of the molten filament through these nozzles.

In this study, CFD analysis was conducted for four different FDM-based 3D printer nozzle designs, evaluating the varying three key parameters: outlet diameter, die angle, and outlet shape using molten ABS as the primary fluid. Ansys Fluent was used for CFD simulations. The impact of these parameters on wall shear stress, pressure drop, and maximum velocity was examined, and the results were carefully interpreted to understand the effects of these parameters on nozzle performance.

2. Methodology

2.1. Material Selection

Ansys Fluent was used as a CFD solver to simulate the material deposition from the different nozzle designs. In Ansys Fluent, the solid material was set to aluminum by default, and material selection for the solid could not be omitted from the specifications since choosing one is required. Therefore, to accurately represent the model, Brass C37700 was selected as the material for the nozzle. The liquid properties of ABS filament at its melting temperature were chosen as the fluid. The properties of ABS are given in Table 1.

2.2. Nozzle Design

The objective of this study was to optimize the geometry of 3D printer nozzles. Various aspects of nozzle geometry needed to be considered. However, a systematic approach to select designs for simulation is essential for minimizing the number of simulations required along with reducing computational costs during design optimization. SolidWorks (Dassault Systèmes, 2011) was used to create different nozzle designs. Figure 1 illustrates the key design parameters of the 3D printer nozzle. The designs vary in die angle, shape, and size, which significantly affect the nozzle's performance[32, 37, 38]. Consequently, four nozzle designs, as shown in Figure 2, were selected to investigate the influence of these parameters on nozzle's performance. A conventional 3D printer nozzle was chosen as the reference (shown on the left), with modifications to its die angle, shape, and size to create Design-1, 2, and 3. This approach enables us to assess the impact of each parameter, aiding in the design of more efficient and manufacturable nozzles by focusing on optimizing the most influential features.

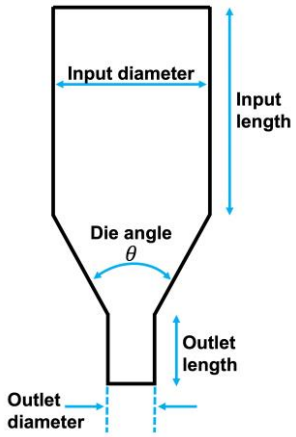

Figure 1. Design parameters of the nozzles.

Table 1. Material properties of the ABS used in the study[39].

Density $(\frac{kg}{m^3})$	Specific Heat Capacity $(\frac{J}{kg} \cdot K)$	Thermal Conductivity $(\frac{W}{m} \cdot K)$	Poisson's Ratio $(-)$	Elastic Modulus (MPa)	Working Temperature $(°C)$	Viscosity $(Pa \cdot s)$
1023	1386	0.2256	0.386	2	240	84

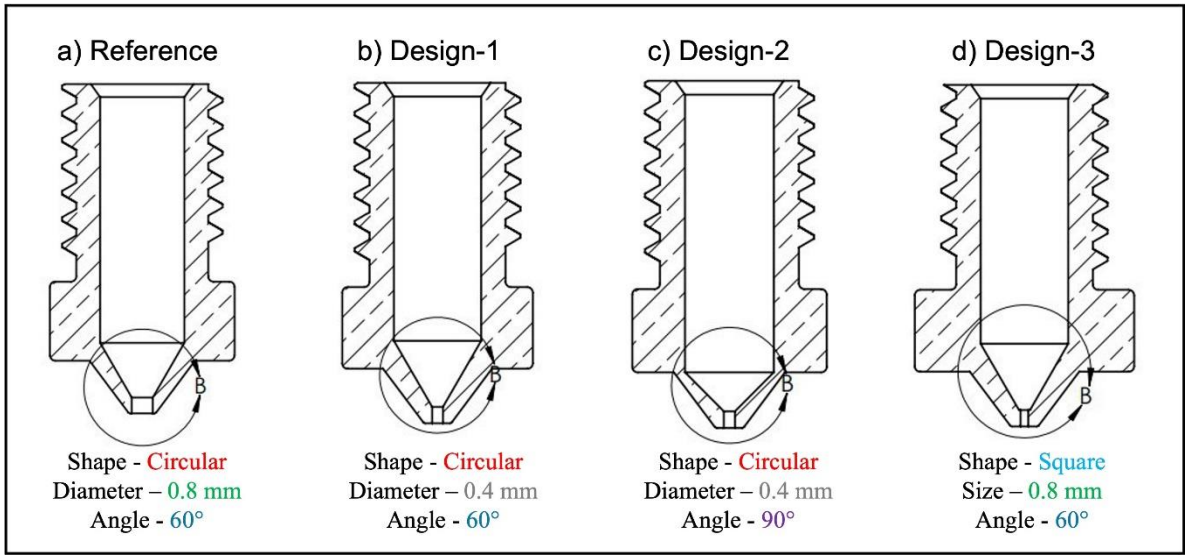

Figure 2. Technical drawing of nozzle designs. a) Reference, b) Design-1, c) Design-2, d) Design-3.

2.3. Simulation Settings

This section discusses the key characteristics of Computational Fluid Dynamics (CFD) analysis that were performed for the fluid flowing through the nozzle. It includes the major stages such as assumptions, meshing, boundary conditions, and simulation setup regarding the analysis.

2.3.1. Assumptions

The operating temperature of the ABS in the liquid state was determined to be 250°C throughout the nozzle. Nevertheless, it is challenging to decide whether non-Newtonian behavior emerges at these elevated temperatures without rheological studies. Further experimental analysis including rheological analysis is required to determine the viscous behavior of the molten ABS under different shear stress values concerning various temperatures. However, based on the observation of maximum shear stress values across the four different nozzle designs, it was assumed that the shear stresses were insufficient to significantly affect the Newtonian behavior of the fluid. Therefore, liquid ABS was considered a Newtonian fluid in this study. The assumption of viscosity being constant with varying shear rates reduces the computational time while introducing a

limitation to the study in terms of accuracy. This limitation can lead to inaccurate representation of the scenarios where shear rates are immense. The potential effect of the significant shear-thinning behavior of the molten filament can result in varying velocity profiles and different pressure distributions throughout the nozzle.

The chosen system for the analysis is an open adiabatic system where only mass flows through the system. Since the temperatures of both the fluid and the solid are constant and equal, there is no heat transfer between the wall and the fluid, making the heat flux equal to zero. This assumption can be considered valid if there is a steady heat source keeping the nozzle's temperature constant, and the filament entering the nozzle is already molten and is in thermal equilibrium with the nozzle.

Flow through the nozzle is considered steady-state flow. The Reynolds numbers for the different outlet designs are calculated based on the following equation:

$$Re = \frac{\rho v d}{\mu} \quad (1)$$

Reynolds number is a dimensionless number that represents the type of flow. In the mentioned equation above, v, ρ, d, and μ are velocity (m/s), fluid density (kg/m^3), outlet diameter (m), and viscosity ($Pa * s$), respectively. According to Cengel and Cimbala[40], flow with $Re < 2300$ is considered to be Laminar. When calculated, the Reynolds Numbers at the inlet in this study for all flows with different nozzle geometries were significantly smaller than 2300. Therefore, it was assumed that the flow throughout the nozzle is Laminar.

In summary of assumptions, the liquid ABS was considered incompressible and Newtonian. Therefore, density and viscosity were constant during the flow throughout the nozzle. The flow was assumed to be in a steady state. Additionally, based on the calculated results of the Reynolds number for each nozzle design, the flow was determined to be laminar. Moreover, the system is in thermal equilibrium given that the temperature of the fluid was set to be equal to the solid's temperature. This condition was achieved by maintaining constant temperatures for both materials. Lastly, the control volume was considered as an open adiabatic system due to no heat exchange across its boundaries. Accurate flow representation limitations that may stem from the assumptions can be attributed to the unknown rheological properties of the molten filament, rather than from the other assumptions mentioned in this section.

2.3.2. Meshing

The meshing process discretizes the object's volume into finite elements. Afterward, the solver software, Ansys Fluent in this study, solves the governing differential equations such as continuity, and Navier-Stokes for each element in the fluid domain. Earlier to meshing, it is crucial to define the boundaries such as inlet, outlet, and wall. These boundaries define the flow domain. Boundaries were specified for three different regions during the internal flow: the inlet surface, the outlet surface, and the wall (Fig. 3). The inlet surface defines the region where the fluid enters the nozzle, and the outlet surface defines the region where the fluid exits. The wall encloses the flow to create an internal flow, with the flowing fluid in contact with the inner surface of the defined wall region. The same meshing technique is applied to the other different nozzle designs in the analysis.

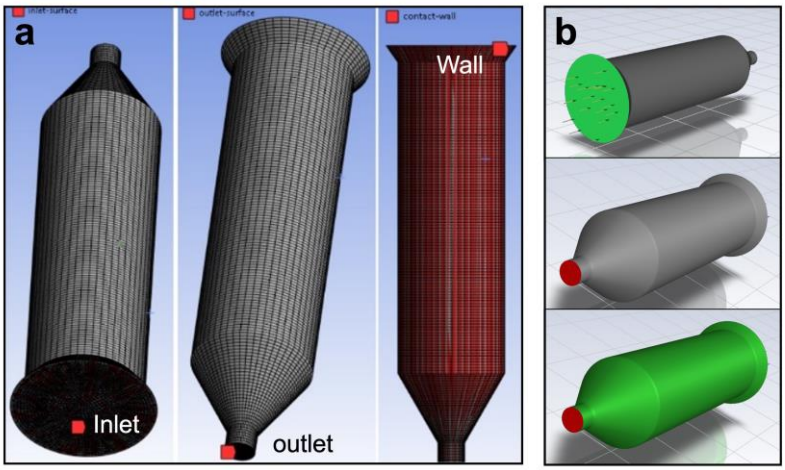

Figure 3. Boundaries of flow in nozzle a) Inlet surface, outlet surface, and wall mesh of the reference nozzle. b) Boundaries of fluid, inlet, outlet, and wall (nozzle inner surface) region.

After defining the boundary regions, meshing was performed with an element size of 8.8314 x 10^{-5} meters. On average, 250,000 nodes were generated during the meshing of each nozzle design. An analysis consisting of 10 different results, including maximum wall shear stress, maximum velocity magnitude, and maximum pressure difference as the number of mesh elements increased, was conducted. Three different figures were plotted to illustrate the fluctuations in results as the number of mesh elements changed. It was observed that significant changes occurred mostly up to 50,000 mesh elements. After 50,000 mesh elements, the results began to stabilize, and the fluctuations minimized. Given that the Ansys Fluent Student version has a limit of 512,000 mesh elements, the 250,000 mesh elements used produced adequate results (Fig. 4).

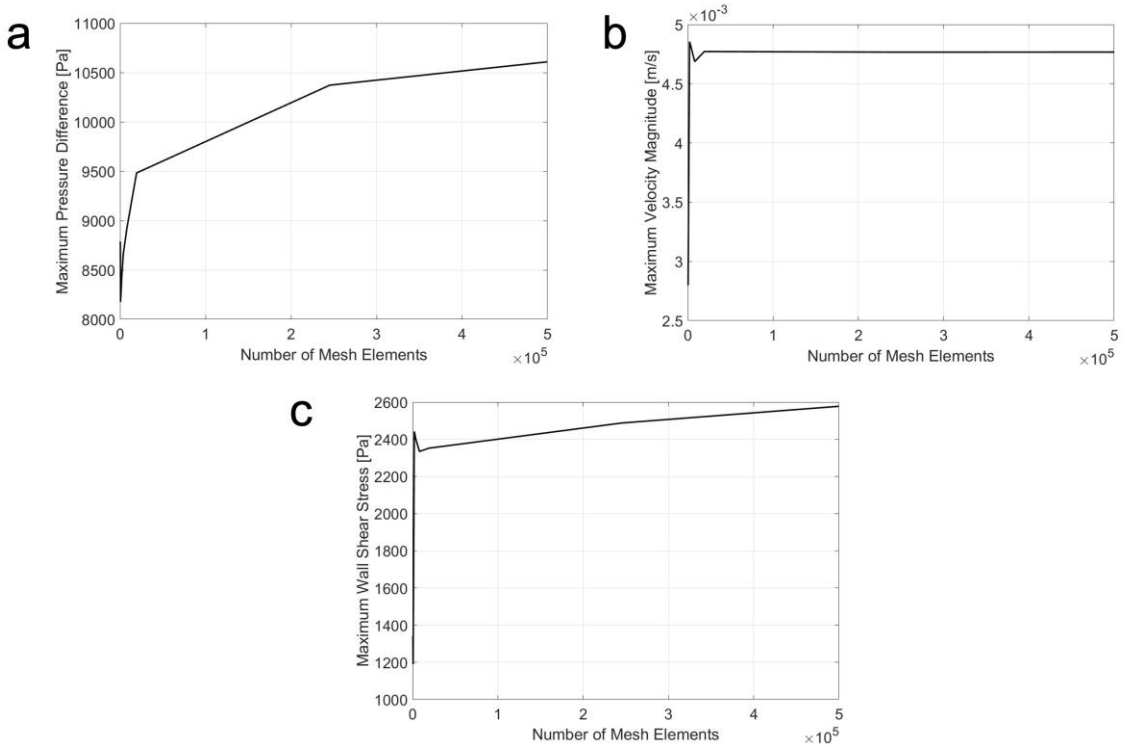

Figure 4. Mesh independence analysis according to the number of elements from 0 to 5 x 10^5. a) Changes in maximum shear stress. b) Changes in maximum velocity magnitude. c) Changes in maximum pressure differences

2.3.3. Boundary Conditions

Defining the boundary conditions in the solver software is one of the fundamental parts of CFD analysis. Boundary conditions involve assigning each solid and fluid material to its corresponding domains and specifying flow and system properties within these defined domains. The boundary conditions applied in the analysis include the conditions at the inlet, outlet, and wall (Fig. 3). Briefly, the definition of this terminology according to the study, Inlet: the region where the fluid enters the nozzle. The flow rate, velocity, or pressure of the entering fluid is specified here. Outlet: the region where the fluid exits the nozzle. The pressure, velocity, or mass flow rate of the exiting fluid is specified here. Wall: the surfaces that enclose the flow, creating an internal flow system. The interactions between the fluid and the wall, such as no-slip conditions, are defined here. These boundary conditions are crucial for accurately simulating fluid behavior and ensuring realistic and reliable results.

The boundary conditions regarding the inlet are specified using a velocity of 0.1 mm/s and a temperature of 503 K. On the other hand, the outlet is set as an outflow with a flow rate weighing 1. Finally, the wall is set as stationary with a no-slip condition and as being adiabatic.

2.3.4. Simulation Setup

During the simulation setup, accuracy was prioritized along with the computational time. Essential software, physical methods, and equations were employed. The solver type was defined as pressure-based, assuming the fluid is incompressible. Discretization methods were selected for accuracy, with strict convergence criteria implemented for continuity and velocities. Ansys Fluent was used as the CFD software package for the simulation. The energy equation was enabled in the physics models

and options of Ansys Fluent. The assumption of no heat transfer between the solid and the fluid implies that conduction heat transfer was not considered, as it was assumed that the solid and fluid were in thermal equilibrium, with negligible heat transfer from the surroundings. The energy equation was enabled to account for any minor changes that might occur during the simulation and to ensure solution stability.

The laminar viscosity model discussed in section 2.3.1 was applied, along with the absolute velocity formulation. The solver type was set to pressure-based with a coupled pressure-velocity coupling scheme. Spatial discretization was performed using a least squares cell-based method for the gradient. Second-order pressure discretization was applied, and both momentum and energy were discretized using a second-order upwind scheme. The time discretization was steady-state, as indicated in the assumptions section. A global time step was used for the pseudo-time method. Residual monitors were set for continuity, x-velocity, y-velocity, z-velocity, and energy, with absolute convergence criteria defined as 0.001 for continuity, x-, y-, and z-velocities, and 10^{-6} for energy.

3. Results and Discussion

This section discusses the results of CFD analysis, including contours and streamlines of various fluid flow properties for each nozzle types. The results also cover wall shear stress, velocity, and pressure values, which will be detailed further in the following sections. As previously mentioned, assumptions, boundary conditions, meshing techniques, convergence criteria, and other simulation settings were kept consistent across all nozzle designs to ensure comparability. Fluid flow properties for each nozzle designs were categorized into five levels: lowest, low, medium, high, and highest. Specifically, minimum and maximum shear stresses on the nozzle's inner wall, the maximum fluid velocity through the nozzle, and the maximum magnitude of pressure drops within the system were analyzed and compared. Before interpreting the results, the way simulations achieved convergence is presented. Figure 5 demonstrates that the solution was considered converged when the residuals dropped below a specific threshold of 10^{-3} for continuity and momentum. Furthermore, the thermal energy monitor remained constant and below the threshold value of 10^{-6} throughout all iterations as anticipated, confirming that no heat transfer analysis was conducted. The convergence criteria were met for all nozzle designs, with the solutions converging on average after 27±8 iterations.

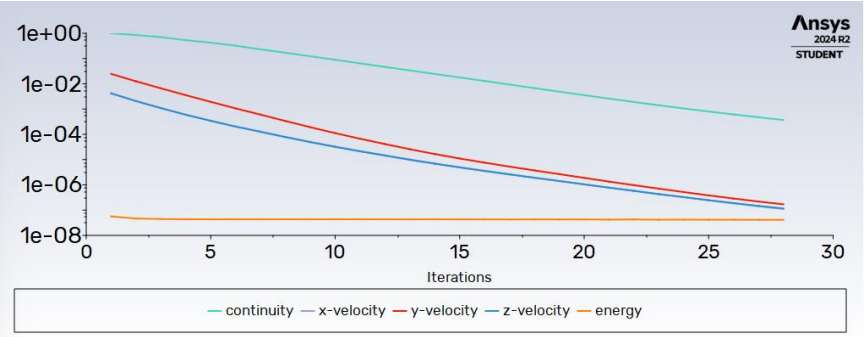

Figure 5. Scaled Residuals Monitor Showing the Convergence for continuity, x-velocity, y-velocity, z-velocity and energy.

Absolute, static, and total pressures were tested in the CFD analysis for all nozzle designs, and as expected, the results for static and total pressures were found to be equivalent. Additionally, it was observed that the pressure differences between the absolute and total pressures were nearly identical. However, the primary goal of including the pressure results in this study is to demonstrate the pressure drop throughout the nozzle, regardless of the pressure type, to accurately observe the effects of nozzle geometry and compare the different designs. Furthermore, the velocity and pressure results are compared to better understand the impact of geometry on performance. Figure 6 illustrates the total pressure values for each region of the various nozzle designs. Negative pressure values can be observed in the Total Pressure Legend. It was anticipated since the initial gauge pressure was set to zero Pascal in the simulation settings. To clarify, when Bernoulli's principle is applied to internal flow within the designed nozzles, it consistently shows that an increase in velocity leads to a decrease in pressure (see Fig. 6). Therefore, observing the negative pressure values in the regions where velocity

increases is understandable. Designs-1 and 2 exhibit higher pressure in the main body compared to the reference and Design-3. This is likely due to their smaller tip diameter (0.4 mm for Design-1 and 2) compared to the 0.8 mm diameter of the reference and size of Design-3. As the flow passes through the nozzle tip in all designs, the pressure gradually decreases until it reaches atmospheric pressure, indicated by the blue color. When comparing Design-1 and Design-2, which have the same outlet diameter, we can observe the effect of the die angle on the pressure drop, as shown in Table 2. Design-2 has a slightly lower pressure drop, despite having a larger die angle. This may be due to the liquid being squeezed through the narrow converging neck in Design-1, which leads to higher pressure.

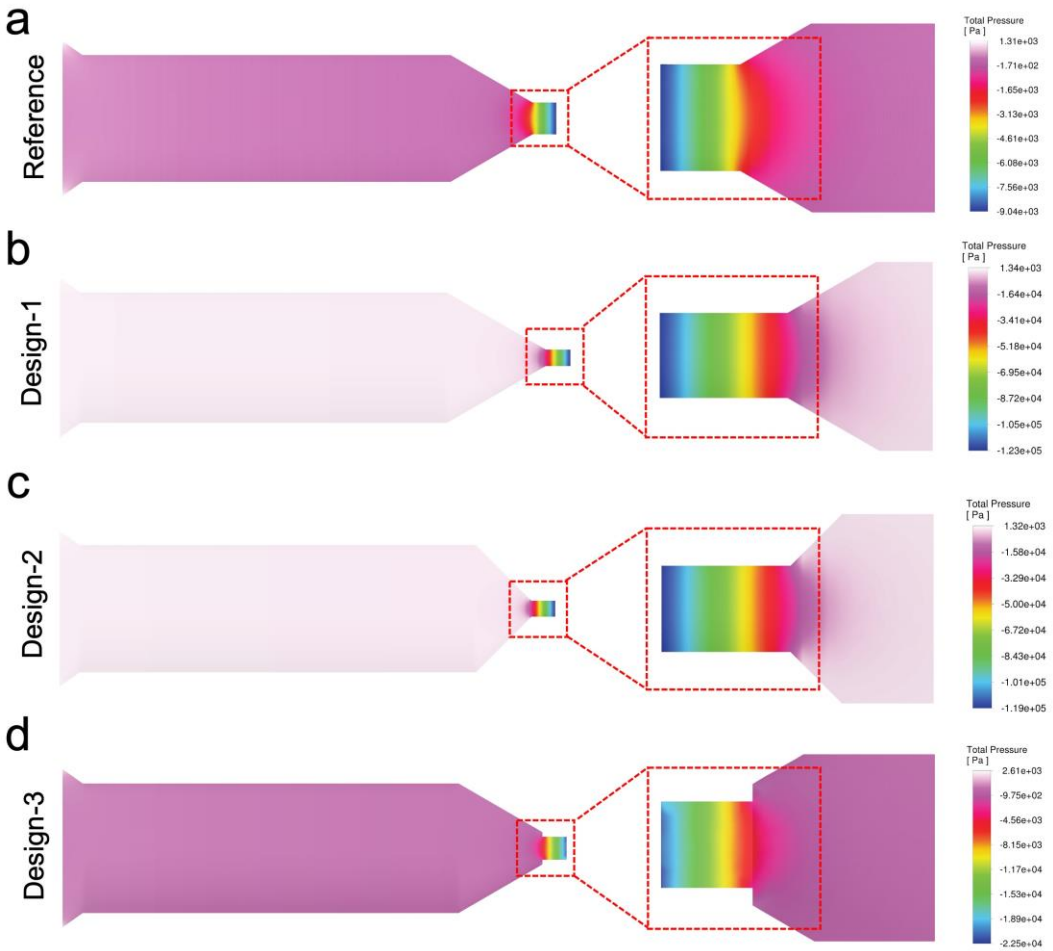

Figure 6. Cross-sectional view of the total pressure magnitude for nozzle designs. a) Reference, b) Design-1, c) Design-2, d) Design-3.

There are no significant differences in the fluid velocity within the main body of all nozzles because the initial velocity of the fluid remains consistent across all designs as seen in the cross-sectional view of the velocity contour results in Figure 7. However, notable changes in fluid velocity occur at the outlet tip, influenced by variations in die angle, outlet diameter, and geometry. For instance, the velocity at the centerline of the reference design is 0.00474 m/s, while it reaches 0.0074 m/s in Design-3, even though both have the same die angle and a very similar outlet area (Table 2). The reference nozzle also maintains the lowest maximum velocity compared to the other designs (Fig. 7), which can be attributed to its largest outlet area. The shear stress at the tip of the surface in the reference design is around $2x10^{-3}$ Pa, whereas in Design-3, it is approximately $1.8x10^{-3}$ Pa, as shown in Figure 8. This suggests that the square shape exerts lower shear stress on the fluid, resulting in higher velocity. Designs-1 and 2 exhibit the same outlet velocity at the centerline, owing to their identical outlet diameters, despite having different die angles. This implies that the die angle does not influence velocity when the diameters are the same. Additionally, Designs-1 and 2 have the highest velocities among the designs due to their smaller outlet areas. Moreover, it is observed that the maximum velocity appears at the centerline of the outlet region for all four nozzle designs.

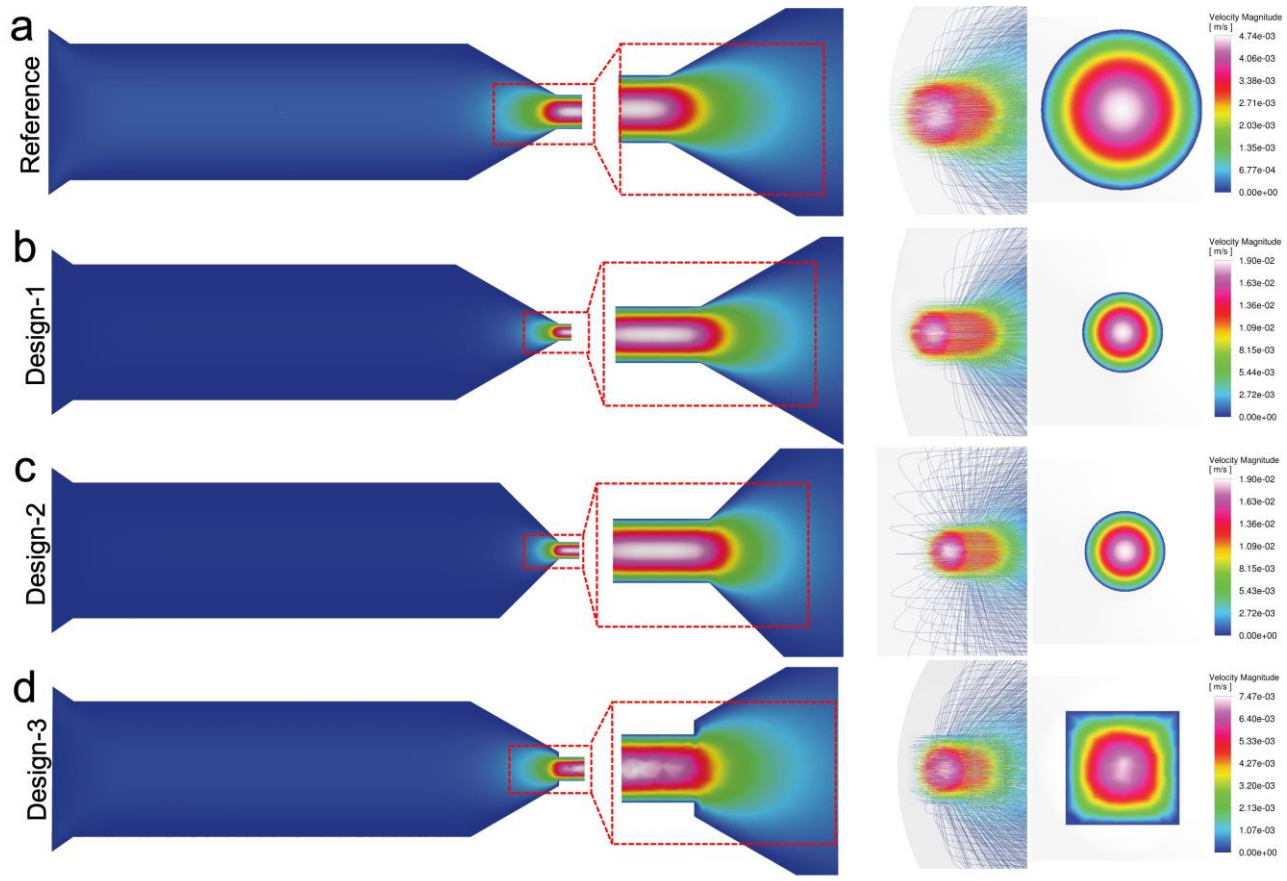

Figure 7. Cross-sectional magnitude, streamline, and frontal view of velocity contour for all nozzle designs. a) Reference, b) Design-1, c) Design-2, d) Design-3.

Table 2. Reynolds number, shear stress, velocity, and pressure drop for the four nozzle designs.

Nozzle	Reynolds Number (Inlet)	Shear Stress (Wall) (Min; Max), (Pa)	Velocity (Max), $\left(\frac{m}{s}\right)$	Pressure Drop (Max. difference), (Pa)
Reference	$4.618 * 10^{-5}$	13.2 ; 2316	0.00474	10345.8
Design-1	$9.256 * 10^{-5}$	12.4 ; 17519	0.0190	123906
Design-2	$9.256 * 10^{-5}$	4.6 ; 18008	0.0190	119859
Design-3	$7.278 * 10^{-5}$	10.0 ; 6438	0.00747	25122

Shear stress plays a crucial role in the performance of 3D printers, particularly in processes like FDM. Higher shear stress within the nozzle reduces the viscosity of the material, improving its flow, which leads to smoother extrusion and better print quality[3, 33].

Design-1 and 2 have almost similar and highest shear stress compared to the reference and Design-4 (Fig. 8). Hence, they can provide better printing quality compared to others. However, if their shear stress is higher than the adequate value, or they have excessive shear stress, it can cause overheating or degradation of the material, negatively affecting the strength and precision of the printing[41]. In the case of excessively low shear stress, the material may not flow properly, resulting in issues like uneven layers[33]. The reference nozzle has the lowest shear stress on the wall compared to the other nozzles (Table 2). This may be due to the reference design's larger outlet area compared to Designs-1 and 2; a smaller outlet area results in higher velocity, which in turn creates higher shear stress. As a result, the melted filament may not be extruded properly, leading to reduced print quality in the reference nozzle compared to the other nozzles. Although Design-3 has the largest outlet area, it experiences slightly

higher shear stress than the reference design due to its square shape. It may provide a similar print quality to the reference nozzle in terms of shear stress, but the square outlet geometry could offer better resolution because of its sharp edges. This might help the layers adhere perfectly without gaps, which may not occur with the curved structure of cylindrical extruded filament. To understand the effect of the die angle on shear stress, Designs-1 and 2 can be compared, as they share the same geometry and diameter but differ in die angles. Design-2 experiences higher shear stress than Design- 1, despite having a larger die angle of 90˚. This can be explained by the fact that the narrowing in Design-1 starts farther from the neck, causing the shear stress distribution to begin farther from the neck as well. In contrast, Design-2 has a less gradual narrowing, meaning the flow is more abruptly squeezed at the neck compared to Design-1. As a result, the larger die angle in Design-2 leads to higher shear stress in the narrowing cylindrical outlet region. Furthermore, the maximum shear stress occurs at the neck of the outlet region in all designs. This is due to the gradual decrease in flow area as the material moves through, reaching the minimum area at the neck. This pattern is also visible in the color spectrum, which ranges from blue (indicating the lowest shear) to white at the neck, where the shear stress is highest. Additionally, improper shear stress levels can increase the risk of nozzle clogging, as the material may not reach a low enough viscosity to maintain a smooth flow. Adequate shear stress is also essential for proper adhesion between layers, which directly influences the structural integrity of the printed object. Balancing shear stress is critical to ensure optimal material flow, layer bonding, and overall printing efficiency[33].

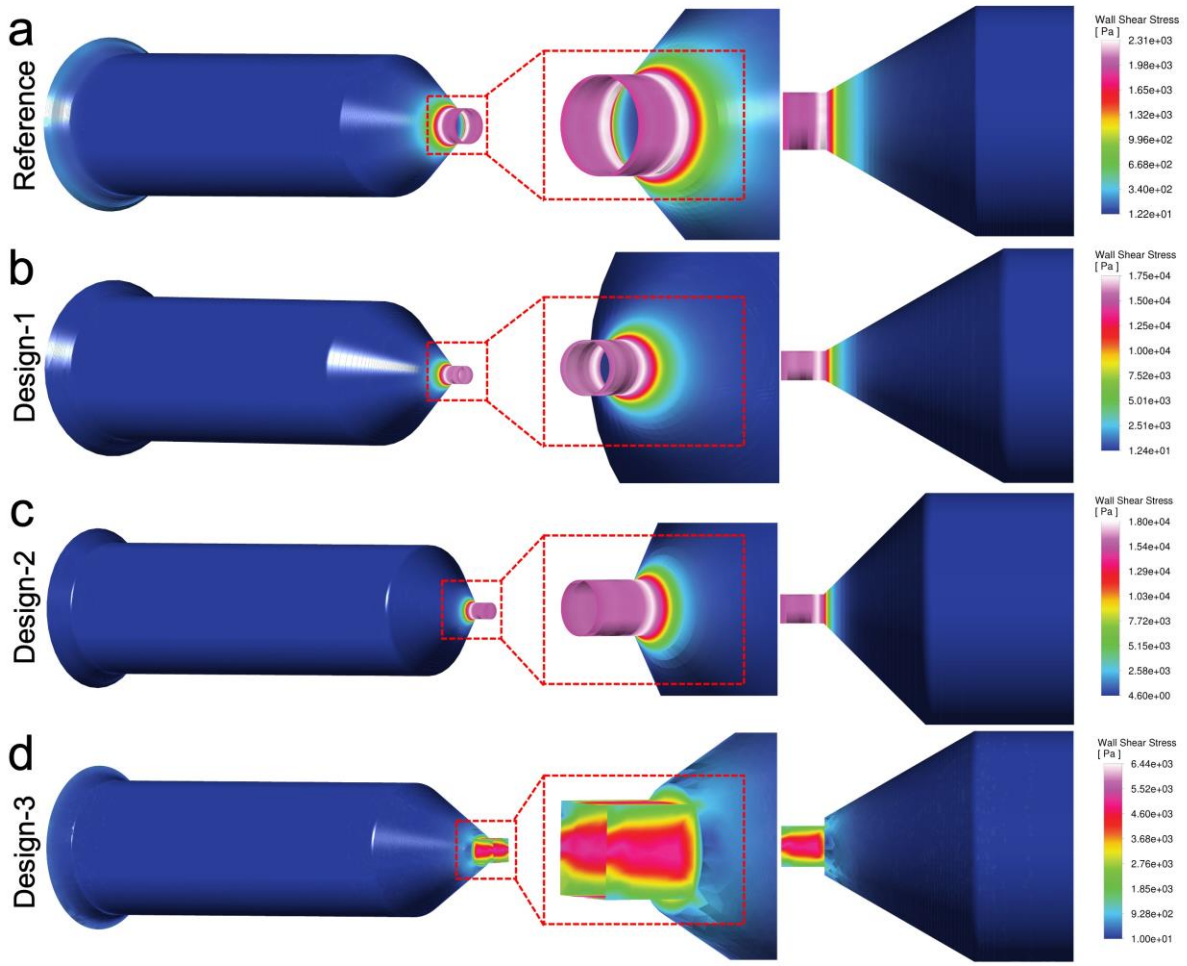

Figure 8. Wall shear stress magnitude throughout the nozzle designs. a) Reference, b) Design-1, c) Design-2, d) Design-3.

4. Conclusion

Consequently, under the specified assumptions and conditions, the CFD analysis of ABS filament in a liquid state flowing through different nozzle designs demonstrated the impact of various nozzle design parameters on system properties. These properties included the shear stress applied by the fluid on the nozzle's inner surface, the fluid velocity profile within the nozzle, and the total pressure variations

throughout the flow. A reduction in the outlet diameter of the reference nozzle led to a significant increase in maximum shear stress, maximum velocity, and the maximum magnitude of pressure drop. On the other hand, an increase in the die angle had a minimal effect on maximum shear stress and no impact on velocity, though it did slightly influence the pressure drop. Modifying the outlet geometry from circular to rectangular caused a moderate increase in shear stress and total pressure drop, with a partial increase in maximum velocity.

Although the manufacturing of the designed nozzles is not a highly challenging task, determining the pressure distribution, velocity profiles, and wall shear stress throughout the nozzle is not experimentally feasible. However, future experimental investigation and validation of the study can be conducted by manufacturing the designed nozzles and operating them in the FDM-based 3-D printer. Necessary sensors and techniques such as high-speed imaging for manufacturing can be employed to validate the CFD results. Alternatively, a feasible validation of this study can be achieved by setting the printing quality and nozzle performance as benchmarks and observing the effects of the study's parameters on these outputs. Thus, the conducted CFD study concerning the effect of nozzle design parameters on essential properties can be validated implicitly in a cost-effective manner. Moreover, future work with experimental analyses can be conducted to address the possible limitations of this study. For instance, rheological analysis can be performed to determine the flow properties of the used molten filament at various temperatures and ensure an accurate Computational Fluid Dynamics (CFD) study.

High shear stress can lead to surface wear. In this case, nozzle material with a high wear resistance should be prioritized. Higher maximum velocity could reduce production time during extrusion. However, the printing quality and cooling time of the extruded material must be inspected carefully when nozzles with higher outlet velocities are used. Moreover, an increase in maximum pressure drops, and correspondingly, an increase in velocity, may contribute to the die-swell in the nozzle. Findings in this study suggest that CFD is an efficient tool for scenarios where experimental research is costly or impractical, to balance nozzle design parameters while meeting printing quality requirements during the use of FDM-based 3D printers.

Acknowledgment

The authors would like to acknowledge Abdullah Gül University for giving an opportunity to work together. We also extend our thanks to Abdurrahman Sivesoğlu for his valuable assistance in the nozzle design.

Contributions of the authors

Conceptualization, M.T.; methodology, visualization, formal analysis, M.T. and R.H.; validation, data curation, writing original draft preparation, M.T. and R.H.; writing review and editing, M.T.; project administration, supervision, M.T. All authors have read and agreed to the published version of the manuscript.

Conflict of Interest Statement

There is no conflict of interest between the authors

Statement of Research and Publication Ethics

The study is complied with research and publication ethics.

References

[1] V. K. Wong and A. Hernandez, "A Review of Additive Manufacturing," *ISRN Mechanical Engineering*, vol. 2012, pp. 1-10, 2012, doi: 10.5402/2012/208760.

[2] N. Shahrubudin, T. C. Lee, and R. Ramlan, "An Overview on 3D Printing Technology: Technological, Materials, and Applications," *Procedia Manufacturing*, vol. 35, pp. 1286-1296, 2019, doi: 10.1016/j.promfg.2019.06.089.

[3] N. Turner, B., Strong, R., & A. Gold, S. (2014). A review of melt extrusion additive manufacturing processes: I. Process design and modeling. Rapid prototyping journal, 20(3), 192-204

[4] A. Waldbaur, H. Rapp, K. Länge, and B. E. Rapp, "Let there be chip—towards rapid prototyping of microfluidic devices: one-step manufacturing processes," (in en), 2011/10/10 2011, doi: 10.1039/C1AY05253E.

[5] M. Lay, N. L. N. Thajudin, A. A. Z. Hamid, A. Rusli, K. M. Abdullah, and K. R. Shuib, "Comparison of physical and mechanical properties of PLA, ABS and nylon 6 fabricated using fused deposition modeling and injection molding," *Composites Part B: Engineering*, vol. 176, p. 107341, 2019, doi: 10.1016/j.compositesb.2019.107341.

[6] E. I. Basri, A. A. Basri, V. N. Riazuddin, S. F. Shahwir, Z. Mohammad, and K. A. Ahmad, "Computational fluid dynamics study in biomedical applications: a review," *International Journal of Fluids and Heat Transfer*, vol. 1, no. 2, pp. 2-14, 2016.

[7] M. H. Zawawi *et al.*, "A review: Fundamentals of computational fluid dynamics (CFD)," *AIP Conference Proceedings*, vol. 2030, no. 1, 2024, doi: 10.1063/1.5066893.

[8] M. M. Aslam Bhutta, N. Hayat, M. H. Bashir, A. R. Khan, K. N. Ahmad, and S. Khan, "CFD applications in various heat exchangers design: A review," *Applied Thermal Engineering*, vol. 32, pp. 1-12, 2012, doi: 10.1016/j.applthermaleng.2011.09.001.

[9] H. H. Hu, "Chapter 10 - Computational Fluid Dynamics," in *Fluid Mechanics (Fifth Edition)*, P. K. Kundu, I. M. Cohen, and D. R. Dowling Eds. Boston: Academic Press, 2012, pp. 421-472.

[10] R. K. Raman, Y. Dewang, and J. Raghuwanshi, "A review on applications of computational fluid dynamics," *International Journal of LNCT*, vol. 2, no. 6, pp. 137-143, 2018.

[11] P. R. Spalart and V. Venkatakrishnan, "On the role and challenges of CFD in the aerospace industry," *The Aeronautical Journal*, vol. 120, no. 1223, pp. 209-232, 2016.

[12] T. Oyinloye and W. Yoon, "Application of Computational Fluid Dynamics (CFD) Simulation for the Effective Design of Food 3D Printing (A Review)," *Processes*, vol. 9, no. 11, p. 1867, 2021, doi: 10.3390/pr9111867.

[13] C.-F. Guo, M. Zhang, and B. Bhandari, "A comparative study between syringe-based and screw-based 3D food printers by computational simulation," *Computers and Electronics in Agriculture*, vol. 162, pp. 397-404, 2019, doi: 10.1016/j.compag.2019.04.032.

[14] M. Temirel, B. Yenilmez, S. Knowlton, J. Walker, A. Joshi, and S. Tasoglu, "Three-Dimensional-Printed Carnivorous Plant with Snap Trap," *3D Printing and Additive Manufacturing*, vol. 3, no. 4, pp. 244-251, 2016, doi: 10.1089/3dp.2016.0036.

[15] T. Glatzel *et al.*, "Computational fluid dynamics (CFD) software tools for microfluidic applications – A case study," *Computers & Fluids*, vol. 37, no. 3, pp. 218-235, 2008, doi: 10.1016/j.compfluid.2007.07.014.

[16] R. Raj, S. V. V. Krishna, A. Desai, C. Sachin, and A. R. Dixit, "Print fidelity evaluation of PVA hydrogel using computational fluid dynamics for extrusion dependent 3D printing - IOPscience," (in en), Text 2022-02-01 2022, doi: doi:10.1088/1757-899X/1225/1/012009.

[17] N. H. Panchal and N. Patel, "ANSYS CFD and experimental comparison of various parameters of a solar still," *International Journal of Ambient Energy*, vol. 39, no. 6, pp. 551-557, 2018, doi: 10.1080/01430750.2017.1318785.

[18] S. O. Alamu, M. J. L. Caballes, Y. Yang, O. Mballa, and G. Chen, "3D Design and Manufacturing Analysis of Liquid Propellant Rocket Engine (LPRE) Nozzle," in *Proceedings of the Future Technologies Conference (FTC) 2019: Volume 2*, 2020: Springer, pp. 968-980.

[19] B. Apacoglu, A. Paksoy, and S. Aradag, "CFD Analysis and Reduced Order Modeling of Uncontrolled and Controlled Laminar Flow Over a Circular Cylinder," *Engineering Applications of Computational Fluid Mechanics*, vol. 5, no. 1, pp. 67-82, 2014, doi: 10.1080/19942060.2011.11015353.

[20] T. Al-Hassan, C. Habchi, T. Lemenand, and F. Azizi, "CFD simulation of creeping flows in a novel split-and-recombine multifunctional reactor," *Chemical Engineering and Processing - Process Intensification*, vol. 162, 2021, doi: 10.1016/j.cep.2021.108353.

[21] A. Tamburini, G. Gagliano, G. Micale, A. Brucato, F. Scargiali, and M. Ciofalo, "Direct numerical simulations of creeping to early turbulent flow in unbaffled and baffled stirred tanks," *Chemical Engineering Science*, vol. 192, pp. 161-175, 2018, doi: 10.1016/j.ces.2018.07.023.

[22] B. Wu and S. Chen, "CFD simulation of non-Newtonian fluid flow in anaerobic digesters," *Biotechnol Bioeng*, vol. 99, no. 3, pp. 700-11, Feb 15 2008, doi: 10.1002/bit.21613.

[23] M. Temirel, S. R. Dabbagh, and S. Tasoglu, "Shape Fidelity Evaluation of Alginate-Based Hydrogels through Extrusion-Based Bioprinting," (in en), *Journal of Functional Biomaterials*, Article vol. 13, no. 4, p. 225, 2022-11-07 2022, doi: 10.3390/jfb13040225.

[24] B. Yenilmez, M. Temirel, S. Knowlton, E. Lepowsky, and S. Tasoglu, "Development and characterization of a low-cost 3D bioprinter," *Bioprinting*, vol. 13, pp. e00044-e00044, 2019.

[25] M. Temirel, C. Hawxhurst, and S. Tasoglu, "Shape Fidelity of 3D-Bioprinted Biodegradable Patches," *Micromachines (Basel)*, vol. 12, no. 2, Feb 13 2021, doi: 10.3390/mi12020195.

[26] A. Malekpour and X. Chen, "Printability and cell viability in extrusion-based bioprinting from experimental, computational, and machine learning views," *Journal of Functional Biomaterials*, vol. 13, no. 2, pp. 40-40, 2022.

[27] M. N. U. Fareez, A. A. S. Naqvi, M. Mahmud, and M. Temirel, "Computational Fluid Dynamics (CFD) Analysis of Bioprinting," *Advanced Healthcare Materials*, 2024, doi: 10.1002/adhm.202400643.

[28] N. Zhang and J. Sanjayan, "Extrusion nozzle design and print parameter selections for 3D concrete printing," *Cement and Concrete Composites*, vol. 137, 2023, doi: 10.1016/j.cemconcomp.2023.104939.

[29] F. Kartal and A. Kaptan, "Investigating the Effect of Nozzle Diameter on Tensile Strength in 3D-Printed Printed Polylactic Acid Parts," (in en), *Black Sea Journal of Engineering and Science*, vol. 6, no. 3, pp. 276-287, July 2023, doi: 10.34248/bsengineering.1287141.

[30] D. Kaplan, S. Rorberg, B. M. Chen, and Y. Sterman, "NozMod: Nozzle Modification for Efficient FDM 3D Printing," in *Proceedings of the 7th Annual ACM Symposium on Computational Fabrication*, ed, 2022.

[31] T. Xu, "Various 3D printing materials with different nozzle design in biomedical area," in *International Conference on Automation Control, Algorithm, and Intelligent Bionics (ACAIB 2022)*, 2022, vol. 12253: SPIE, pp. 445-453.

[32] "3D Printer Nozzle Design and Its Parameters: A Systematic Review | SpringerLink," 2024, doi: 10.1007/978-981-15-2647-3_73.

[33] D. R. Ian Gibson , Brent Stucker, *Additive Manufacturing Technologies: 3D Printing, Rapid Prototyping, and Direct Digital Manufacturing | SpringerLink*. Springer, 2015.

[34] H. Zhang, L. Zhang, H. Zhang, J. Wu, X. An, and D. Yang, "Fibre bridging and nozzle clogging in 3D printing of discontinuous carbon fibre-reinforced polymer composites: coupled CFD-DEM modelling," *The International Journal of Advanced Manufacturing Technology*, vol. 117, no. 11-12, pp. 3549-3562, 2021, doi: 10.1007/s00170-021-07913-7.

[35] H. Zong *et al.*, "Simulation of printer nozzle for 3D printing TNT/HMX based melt-cast explosive," (in En), *The International Journal of Advanced Manufacturing Technology*, OriginalPaper vol. 119, no. 5, pp. 3105-3117, 2022-01-05 2022, doi: doi:10.1007/s00170-021-08593-z.

[36] B. Alphonse, R. Basavaraj, H. Koten, R. Balasubramanian, and S. Umrao, "Comparative design and CFD analysis of 3-D printed acrylonitrile butadiene styrene nozzle aerator for discharge reduction," *Thermal Science*, vol. 26, no. 2 Part A, pp. 857-869, 2022, doi: 10.2298/TSCI201114155A.

[37] O. Hıra, S. Yücedağ, S. Samankan, Y. Ö. Çiçek, and A. Altınkaynak, "Numerical and experimental analysis of optimal nozzle dimensions for FDM printers," *Progress in Additive Manufacturing*, 2022, doi: 10.1007/s40964-021-00241-y.

[38] B. Lizenboim, S. Kenig, and N. Naveh, "The Effect of Nozzle Geometry on the Structure and Properties of 3D Printed Carbon Polyamide Composites," *Applied Composite Materials*, vol. 31, no. 1, pp. 83-99, 2024, doi: 10.1007/s10443-023-10166-0.

[39] S. Han, Y. Xiao, T. Qi, Z. Li, and Q. Zeng, "Design and Analysis of Fused Deposition Modeling 3D Printer Nozzle for Color Mixing," *Advances in Materials Science and Engineering*, vol. 2017, pp. 1-12, 2017, doi: 10.1155/2017/2095137.

[40] Y. Cengel and J. Cimbala, *Ebook: Fluid mechanics fundamentals and applications (si units)*. McGraw Hill, 2013.

[41] Q. Sun, G. M. Rizvi, C. T. Bellehumeur, and P. Gu, "Effect of processing conditions on the bonding quality of FDM polymer filaments," *Rapid Prototyping Journal*, vol. 14, no. 2, pp. 72-80, 2008, doi: 10.1108/13552540810862028.

[42] A. L. Rutz, K. E. Hyland, A. E. Jakus, W. R. Burghardt, and R. N. Shah, "A multimaterial bioink method for 3D printing tunable, cell-compatible hydrogels," *Advanced Materials*, vol. 27, no. 9, pp. 1607-1614, 2015.

[43] N. Hasan and Y. B. Mathur, "Optimizing the Design of Earth Air Tunnel Heat Exchanger for Cooling in Summer Season," *International Multidisciplinary Mulitilingual E-Journal*, vol. 5, no. 1, pp. 19-29.